Microscopy and Microanalysis, **31** (7), 2025, 2018–2020
https://doi.org/10.1093/mam/ozaf048.1005

Microscopy AND Microanalysis

Proceedings

Microstructure, Microhardness and Corrosion Behavior of a High Entropy Heat Treated Alloy

Cristina Jiménez-Marcos[1], Santiago Brito-García[1], Julia Claudia Mirza-Rosca[1,2,*], and Ionelia Voiculescu[3]

[1]*Department of Mechanical Engineering, University of Las Palmas de Gran Canaria, Las Palmas de Gran Canaria, Spain.*
[2]*Materials Engineering and Welding Department, Transilvania University of Brasov, Brasov, Romania*
[3]*Faculty of Industrial Engineering and Robotics, Politehnica University of Bucharest, Bucharest, Romania*

*Corresponding author: julia.mirza@ulpgc.es

The exceptional mechanical strength, corrosion resistance and thermal stability of High Entropy Alloys (HEAs) have made them a preferable substitute for traditional materials. They are very beneficial for applications in harsh situations because of these qualities. The CoCrFeMnNi alloy has been extensively researched among HEAs due of its well-balanced hardness and strength characteristics. However, its performance can be further improved by thermal processing and compositional changes.

Generally, the addition of Mo refines the microstructure, hardness, and corrosion resistance of CoCrFeMoNi alloys, as molybdenum is normally used in alloys for strength improvement [1]. During such addition, a fine microstructure should be developed, since these attributes enable the alloy to serve in extreme environments. The heat treatment of the alloy is also considered vital for the optimization of electrochemical and mechanical properties along with hardness.

The present work investigates the effects of heat treatment and posterior cooling at room temperature of CoCrFeMoNi alloys for industrial application. In this work, scanning electron microscopy, SEM, will be used for structural microanalysis; Vickers hardness test will be performed and electrochemical tests will be carried out.

The HEA CoCrFeMoNi ingot was first heat treated in a Hobersal Mod 12-PR/300 electric muffle furnace at 800°C for 2 hours and then cooled to room temperature. A Buehler IsoMet 4000 precision saw was used to separate the HEA ingot into separate pieces for the microstructural, electrochemical, and nanoindentation testing. A phenolic resin was subsequently used to embed the HEA sample through the hot mounting step. After utilizing the Struers TegraPol-11 polisher with progressive silicon carbide papers ranging from 400 to 2000 grit, the samples were ground and polished. 0.1-micron alpha alumina suspension polishing cloths were then used to achieve a mirror finish (see to Fig. 1) [2].

A Hitachi TM3030 scanning electron microscope with an EDX spectrometer (Hitachi High-Tech Science Corporation, Tokyo, Japan) was used for SEM observations, with a voltage set at 15 kV and a working distance of 10.7 mm. Ten measurements are taken by the use of Future Tech FM-810 hardness tester applying a load of 200 gf. To determine the corrosion rate, as well as to perform electrochemical impedance spectroscopy (EIS), direct and alternating current electrochemical experiments were carried out using the BioLogic Essential SP-150 potentiostat, the electrochemical cell and a 3.5 % NaCl salt solution at room temperature.

The HEA sample showed a compact dendritic microstructure without cracking as shown in Fig. 2a. A semi-quantitative analysis was carried out to determine the chemical composition of the samples studied, where points 1, 2 and 3 indicate dendritic zones and points 4, 5 and 6 indicate interdendritic zones on the surface of the sample, as shown in Fig. 2b. Fig. 2c. shows the EDS spectra generated in addition to the wt% and at% values, where it can be seen that the zones are rich in molybdenum, while the dendritic zones presented high values of iron, cobalt and nickel. On the other hand, they showed similar values of chromium.

After 10 Vickers hardness measurements, a mean hardness of 382.50 HV with a standard deviation of 0.60 was obtained.

Electrochemical tests, particularly corrosion rate tests, show that the value obtained of $2.41 \cdot 10^{-2}$ mmpy are higher than those obtained in previous tests with [3] or without heat treatment [4,5].

A quasi-capacitive response, characterized by an incomplete semicircle, was detected in the Nyquist diagram. The Bode-impedance and Bode-phase diagrams indicate slightly low impedance and phase angle values (see Fig. 3c and Fig. 3d, respectively). The equivalent circuit that best fits the HEA is $R_e(Q_1(R_1(Q_2R_2))$, where R_e is the dissolution resistance, Q_1 and R_1 are the phase constant element and the resistance of the passive porous layer of the sample surface and Q_2 and R_2 are the phase constant element and the resistance of the passive compact layer (see Fig. 4).

The HEA sample exhibits a dense dendritic microstructure free of any discernible fissures. Dendritic zones are rich in iron, cobalt, and nickel, whereas interdendritic zones are rich in molybdenum; chromium content is similar in both zones. The sample exhibits an average Vickers hardness of 382.50 HV, accompanied by a minimal standard variation of 0.60 HV, signifying stable hardness. The determined corrosion rate ($2.41 \cdot 10^{-2}$ mmpy) exceeds that of other investigations without heat treatment. EIS analysis suggests a quasi-capacitive response with a passive layer with a porous extern part and a passive compact intern layer.

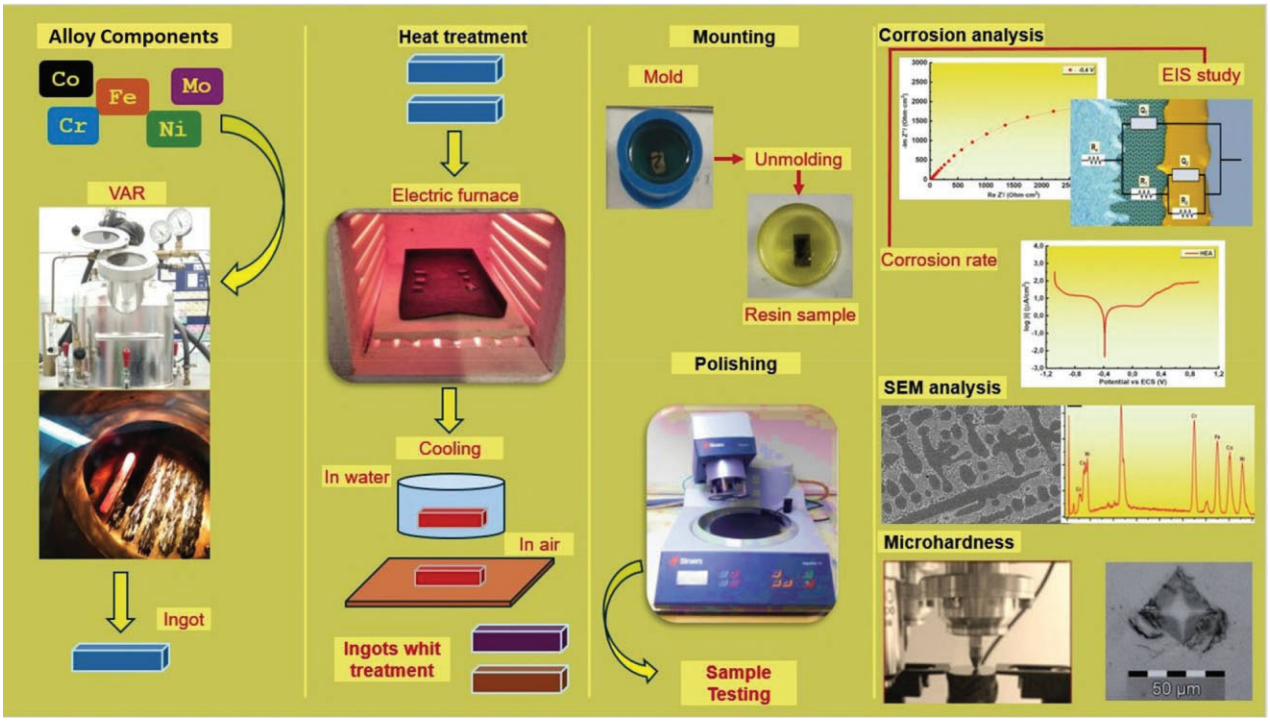

Fig. 1. Preparation of the sample that will be studied.

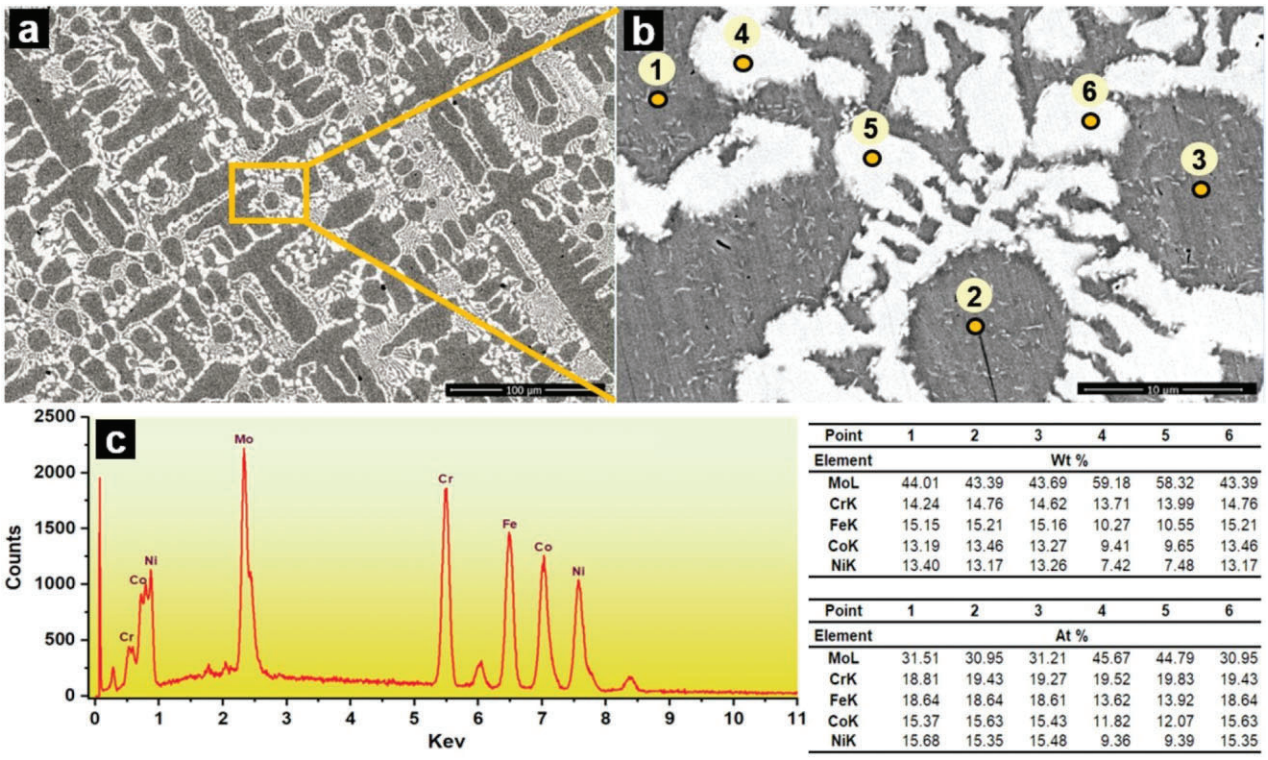

Point	1	2	3	4	5	6
Element			Wt %			
MoL	44.01	43.39	43.69	59.18	58.32	43.39
CrK	14.24	14.76	14.62	13.71	13.99	14.76
FeK	15.15	15.21	15.16	10.27	10.55	15.21
CoK	13.19	13.46	13.27	9.41	9.65	13.46
NiK	13.40	13.17	13.26	7.42	7.48	13.17

Point	1	2	3	4	5	6
Element			At %			
MoL	31.51	30.95	31.21	45.67	44.79	30.95
CrK	18.81	19.43	19.27	19.52	19.83	19.43
FeK	18.64	18.64	18.61	13.62	13.92	18.64
CoK	15.37	15.63	15.43	11.82	12.07	15.63
NiK	15.68	15.35	15.48	9.36	9.39	15.35

Fig. 2. SEM image (a)), SEM image with the selected points (b)) and EDS spectra and composition (c)) of the sample.

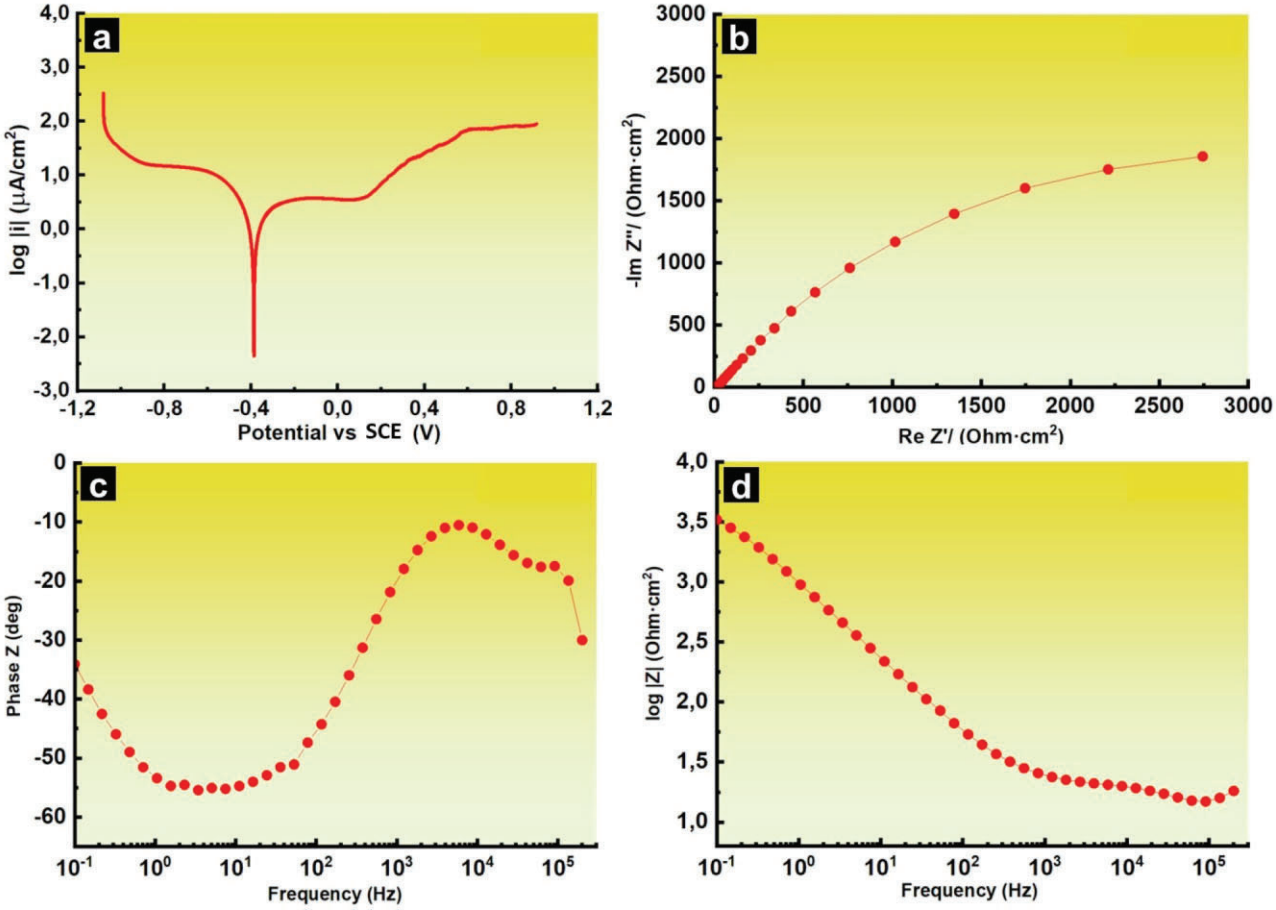

Fig. 3. Corrosion rate (a)), Nyquist diagram (c)), Bode-impedance diagram (c)) and Bode-phase diagram (d)) of the sample.

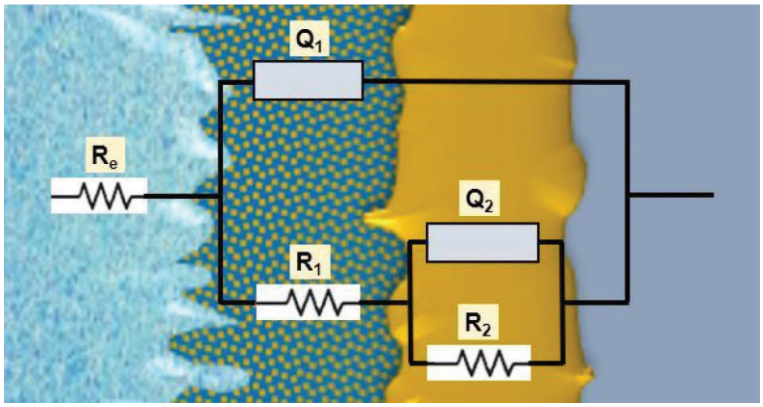

Fig. 4. Electrical equivalent circuit $R_e(Q_1(R_1(Q_2R_2))$.

References

1. Dong Z *et al. Materials (Basel)*. (2021) **14**, 1–16 doi:10.3390/ma14051073.
2. Brito-Garcia SJ *et al. Metals (Basel)*. (2023) **13**, **854** doi:10.3390/met13050854.
3. Liu N *et al. Mater. Sci. Technol*. (2023) **39**, 2782–2791 doi:10.1080/02670836.2023.2225904.
4. Brito-Garcia S *et al. Mater*. (2023) **16** 5, 1832 doi:10.3390/MA16051832
5. Brito-Garcia SJ *et al. Metals (Basel)*. (2023) **13**, **883** doi:10.3390/met13050883